IEEE Photonics Journal
An IEEE Photonics Society Publication

Open Access

Beam Size Optimization and Adaptation for High-Altitude Airborne Free-Space Optical Communication Systems

Volume 11, Number 2, April 2019

Vuong V. Mai, *Member, IEEE*
Hoon Kim, *Senior Member, IEEE*

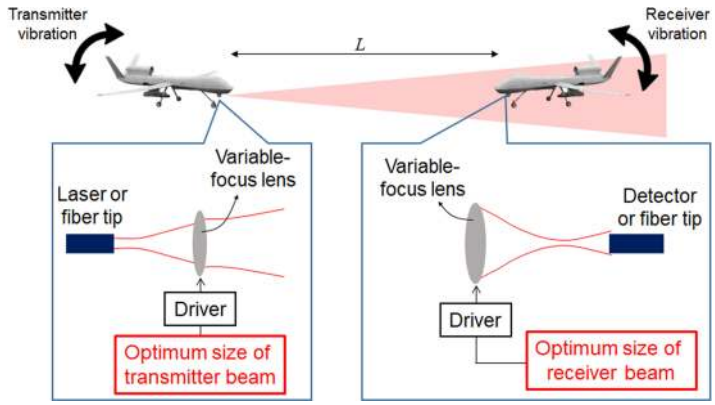

DOI: 10.1109/JPHOT.2019.2901952
1943-0655

IEEE photonics SOCIETY

IEEE

Beam Size Optimization and Adaptation for High-Altitude Airborne Free-Space Optical Communication Systems

Vuong V. Mai, *Member, IEEE*, and Hoon Kim, *Senior Member, IEEE*

School of Electrical Engineering, Korea Advanced Institute of Science and Technology, Daejeon 34141, South Korea

DOI:10.1109/JPHOT.2019.2901952

Manuscript received February 19, 2019; accepted February 24, 2019. Date of publication February 27, 2019; date of current version March 13, 2019. This work was supported by the Future Combat System Network Technology Research Center program of Defense Acquisition Program Administration and Agency for Defense Development (UD160070BD). Corresponding author: Hoon Kim (e-mail: hoonkim@kaist.ac.kr).

Abstract: High-altitude airborne platforms interconnected by free-space optical communications (FSOCs) have recently emerged as a promising solution for establishing wireless networks for rural and remote areas. The performance of FSOC system is severely degraded by the angle-of-arrival (AoA) fluctuation and pointing error. The precise alignment between the optical transmitter and receiver can be achieved by using the pointing, acquisition, and tracking (PAT), but it should work within the tight constraints of airborne platforms on size, weight, and power. It is also highly desirable that the PAT operates rapidly (e.g., without iteration for optimization) since the airborne platforms can be on the fast move. We propose a rapid and computation power-efficient adaptive beam control technique, where the beam sizes are adjusted without iterations at both the transmitter and receiver using nonmechanical variable-focus lenses, to mitigate the deleterious effects of AoA fluctuation and pointing error simultaneously. For this purpose, we provide the closed-form expressions about the optimum beam sizes at the transmitter and receiver for the outage probability. We carry out Monte Carlo simulations to validate the accuracy of our theoretical derivations. We show that the airborne FSOC system using the adaptive beam control technique outperforms the system having fixed beam sizes over wide ranges of AoA fluctuation and pointing error.

Index Terms: Angle-of-arrival fluctuation, free-space optical communication, pointing error.

1. Introduction

Free-Space optical communications (FSOCs), thanks to their capability to transport high-speed data over long distances without exhausting RF resources, have recently drawn a great deal of interest for wireless communications between airborne platforms operating at high altitudes [1]–[6]. For example, Google and Facebook launched Project Loon and Project Aquila, respectively, in a bid to provide internet service down to rural and remote areas by interconnecting balloons or drones flying in the stratosphere using the FSOC technology [5], [6]. At such high altitudes, the density of air is so thin that the impacts of atmospheric turbulence on the performance of FSOC systems are negligible compared to at the ground level. It is also free from weather events (e.g., fog, rain, and clouds) at those altitudes. Thus, the major technical challenge associated with the FSOC system

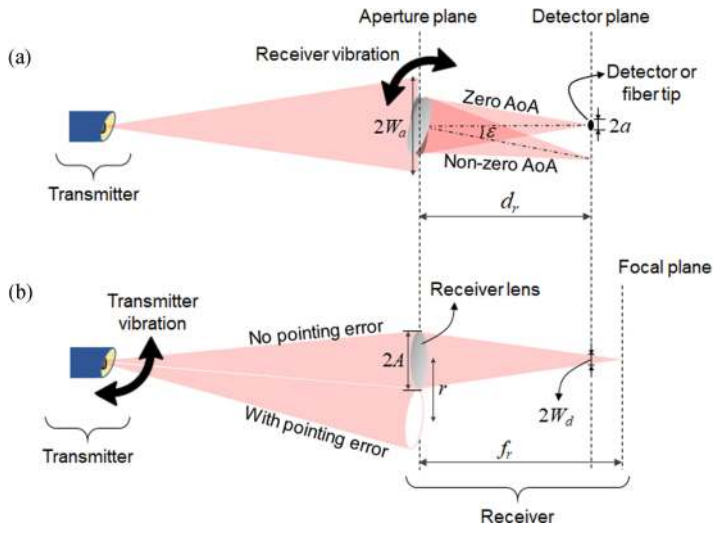

Fig. 1. (a) AoA fluctuation and (b) pointing error.

operating in the stratosphere is the precise alignment between the transmitter and receiver. The errors in alignment can be categorized into angle-of-arrival (AoA) fluctuation and pointing error (see Fig. 1). AoA fluctuation can be caused by the vibration at the receiver and the wavefront tilt of optical signal after passing through a turbulent channel. They manifest themselves as spot motion or image dancing at the focal plane of the receiver. On the other hand, transmitter vibrations and beam wandering give rise to pointing errors. The net effect of pointing error is the beam wandering on the aperture plane (of the receiver). Since these alignment errors introduce random attenuations of the detected signal, they severely degrade the performance of FSOC systems. Thus, it is very important to analyze the performance of FSOC system under the effects of both AoA fluctuation and pointing error. The results of the analysis can be used to improve the system performance. It should be noted that if we develop any technique to improve the system performance, it should work within tight constraints of airborne platforms on size, weight, and power (SWaP). It is also highly desirable that the technique operates rapidly (e.g., without iteration for optimization) since the airborne platforms can be on the fast move.

There are numerous works on the performance analysis of FSOC system [7], [8]. In most of the works, it was assumed that both the transmitter and receiver were stationary and the receiver had a large field of view (FoV). Thus, they took into consideration only the effects of pointing error (neglecting the effects of AoA fluctuation). However, high-speed FSOC systems typically employ small-area detectors (or fiber tips), which provide the wide electrical bandwidth and also reduce the effect of ambient light. Thus, it would be quite challenging to focus the received light on the detector in the presence of AoA fluctuation. Recently, there has been an increased interest in the performance analysis of FSOC systems under the effect of AoA fluctuation [9]–[12]. A 1.28-Tb/s FSOC system utilizing single-mode fiber (SMF) at the receiver was experimentally demonstrated in [9], where one-day measurements of AoA fluctuation and its impact on bit-error rate (BER) performance were reported. The AoA fluctuation-induced link loss was modeled theoretically in [10]. Based on the model, the outage probability of terrestrial FSOC systems was analyzed for both the coherent and direct-detection receivers. In [11], the mathematical models of mixing efficiency and BER in the heterodyne detection were derived for ground-to-air FSOC systems in the presence of AoA fluctuation. However, the last two works did not provide the probability density function (PDF) or cumulative density function (CDF) of the link loss induced by AoA fluctuation and pointing error. Very recently, the study on these PDF and CDF has been presented in [12]. Also provided in this study was an analytical expression about the outage probability of low-altitude airborne FSOC systems. However, the AoA fluctuation-induced loss is oversimplified by the assumptions that (i)

there is no detected light when AoA is outside of the receiver's FoV and (ii) there is no loss in light power when AoA is within the receiver's FoV. Moreover, no closed-form expressions about the optimum system performance have been derived in the previous works. Without closed-form expressions, the analysis would require considerable amounts of computational time and power consumption, and thus might not be applicable to airborne FSOC systems having tight SWaP constraints.

In addition to those performance analyses, there have been several studies on the mitigation of AoA fluctuation at the receiver [13]–[15]. For example, the instantaneous beam position on the focal plane [i.e., a plane perpendicular to the axis of a lens and located at the focus of the received light, as shown in Fig. 1(b)] was detected by using an optical sensor, and a fast-steering mirror (FSM) was utilized to correct the beam displacement. This technique was utilized through theory and experiment to improve the fiber coupling efficiency in a satellite-to-ground communication system [13]. The BER improvement of coherent detection by applying the same technique was also investigated for an inter-satellite FSOC [14]. In another work, a two-dimensional fiber positioner was used to track the focused beam on the focal plane [15]. However, all these techniques rely on mechanical positioning systems (i.e., FSM or fiber positioner), which would not be desirable to airborne FSOC systems due to tight SWaP constraints. Moreover, those positioning systems are prone to mechanical failure and suffer from the limitation of precise control. For pointing errors, it has been shown that the performance degradation can be mitigated by adaptive beam control techniques, where the transmitter beam size is adjusted adaptively to the system environment (e.g., transmission distance) [16], [17]. A comprehensive survey and operations of this technique can be found in [17]. However, one of the limitations of existing techniques is that AoA fluctuation and pointing error are studied separately; thus, none of them is able to cope with both impairments simultaneously.

Hence, we present the performance analysis and improvement of airborne FSOC system in the presence of both AoA fluctuation and pointing error. The main contributions of this work are as follows:

i. We first improve the theoretical model of AoA fluctuation-induced link loss by using Gaussian approximation. Based on the model, we derive the PDF and CDF of link loss induced by AoA fluctuation and pointing error. We then provide the closed-form expressions about the outage probability and optimum beam sizes for outage probability. The accuracy of our theoretical derivations are evaluated by using the Monte Carlo simulation.
ii. The other contribution of this work is that we propose an adaptive beam control technique, where the beam sizes at both transmitter and receiver are adjusted optimally for the outage probability in the presence of both AoA fluctuation and pointing error. To the best of our knowledge, this is the first technique to deal with both impairments simultaneously, compared with previous compensation techniques of AoA fluctuation [13]–[15] and pointing error [16], [17]. The technique was introduced briefly in our recent study [18], yet there was a lack of practical guidance on how to implement it. We provide in this paper the practical guidance on system design and operation. The major benefits of the proposed technique include that it can be implemented simply, for example, by using variable-focus lenses. The non-mechanical implementation of this technique enhances its reliability. Also, it reduces the SWaP of the transmitter and receiver considerably, and thus makes it suitable for airborne applications. To realize the proposed technique in an energy-efficient manner, we utilize the closed-form expressions about optimum beam sizes. They not only eliminate the time-consuming iteration process of optimization, but also save the computational power (required for the optimization) for low SWaP and fast-tracking applications.

The remainder of this work is organized as follows. In Section 2, the PDF and CDF of link loss induced by the AoA fluctuation and pointing error are newly developed using Gaussian approximation. Next, we present closed-form expressions about optimum beam sizes and the adaptive beam control technique in Section 3. The accuracy of analysis and the effectiveness of the adaptive beam control technique are discussed in Section 4. Lastly, Section 5 concludes our work.

2. Link Loss Models

Fig. 1 illustrates the system impairments caused by AoA fluctuation and pointing error. Firstly, the receiver vibrations introduce AoA fluctuations which degrade the power received by the detector. Secondly, due to the pointing errors caused by transmitter vibrations, the beam footprint at the aperture plane deviates from the center of the receiver aperture, which directly reduces the received power. In this paper, we focus on high-altitude airborne FSOC systems, where the transmission distance is typically long, e.g., tens of km. Therefore, the effect of transmitter vibrations on AoA fluctuations can be neglected by making far-field assumptions. These assumptions have been commonly used in previous studies of AoA fluctuations [10].

2.1 AoA Fluctuation-Induced Link Loss

The AoA, defined as the incidence angle of optical signal relative to the receiver aperture plane, is denoted as ε in Fig. 1(a). We consider this angular deviation in vertical and horizontal directions. As commonly assumed in literature [10], [12], the vertical (ε_v) and horizontal (ε_h) AoA fluctuations can be regarded as independent and identically distributed (iid) zero mean Gaussian random variables with variance σ_ε, i.e., $\varepsilon_v \sim N(0, \sigma_\varepsilon)$ and $\varepsilon_h \sim N(0, \sigma_\varepsilon)$. Therefore, the total radial AoA ε, given by $\varepsilon = (\varepsilon_v^2 + \varepsilon_h^2)^{1/2}$, can be modeled by a Raleigh distribution, where the scale parameter of the distribution is the standard deviation of AoA fluctuation σ_ε. The PDF of AoA fluctuation is given by

$$PDF_\varepsilon(\varepsilon) = \frac{\varepsilon}{\sigma_\varepsilon^2} \exp\left(-\frac{\varepsilon^2}{2\sigma_\varepsilon^2}\right) \tag{1}$$

where σ_ε is the standard deviation of AoA fluctuation. For a thin lens having a circular aperture at the receiver, the intensity of the diffracted beam pattern at the detector plane can be expressed by using the Airy pattern as

$$I(x, y) = \frac{P_0\pi}{4\lambda^2 N^2}\left(\frac{2J_1\left(\frac{\pi}{\lambda N}\sqrt{(x - d_r\varepsilon)^2 + y^2}\right)}{\frac{\pi}{\lambda N}\sqrt{(x - d_r\varepsilon)^2 + y^2}}\right)^2 = \frac{P_0\pi}{4(W_r/1.22)^2}\left(\frac{2J_1\left(\frac{\pi}{W_r/1.22}\sqrt{(x - d_r\varepsilon)^2 + y^2}\right)}{\frac{\pi}{W_r/1.22}\sqrt{(x - d_r\varepsilon)^2 + y^2}}\right)^2 \tag{2}$$

where P_0 is the total power incident on the aperture, λ is the optical wavelength, N is the f-number, $W_r = 1.22\lambda N$ is the radius of Airy pattern (i.e., the radius of the first dark ring) on the detector plane, and d_r is the distance between aperture and detector planes, J_1 (.) is the Bessel function of the first kind of order one, and (x, y) is the vector position in the detector plane. Then, the link loss induced by AoA fluctuation can be calculated as the fraction of power collected by the circular detector (having a diameter of $2a$) to the total power incident. Thus, it can be written as

$$h_{AoA}(\varepsilon) = \frac{\pi}{4(W_r/1.22)^2}\int_{-a}^{a}\int_{-\sqrt{a^2-x^2}}^{\sqrt{a^2-x^2}}\left(\frac{2J_1\left(\frac{\pi}{W_r/1.22}\sqrt{(x - d_r\varepsilon)^2 + y^2}\right)}{\frac{\pi}{W_r/1.22}\sqrt{(x - d_r\varepsilon)^2 + y^2}}\right)^2 dxdy \tag{3}$$

Unfortunately, there is no closed-form expression about (3). Hence, we utilize a Gaussian pattern as an alternative model of the diffracted beam, which is expressed as

$$I(x, y) \approx \frac{\pi}{2W_d^2}\exp\left(\frac{-\left\{(x - d_r\varepsilon)^2 + y^2\right\}}{2W_d}\right) \tag{4}$$

Here, W_d is the equivalent radius of Gaussian beam (where the intensity drops by a factor of e^{-2}) on the detector plane. It is found that this approximation is accurate when the radius of Gaussian beam is about one-third the Airy disk radius, i.e., $W_d \approx W_r/3$ [19]. Utilizing (4), we derive the following

approximation of the AoA fluctuation-induced link loss as

$$h_{AoA}(\varepsilon) \approx \frac{\pi}{2{W_d}^2} \int_{-a}^{a} \int_{-\sqrt{a^2-x^2}}^{\sqrt{a^2-x^2}} \exp\left(\frac{-\left\{(x-d_r\varepsilon)^2+y^2\right\}}{2W_d}\right) dxdy \approx \frac{2a^2}{{W_d}^2} \exp\left(\frac{-2(d_r\varepsilon)^2}{{W_d}^2}\right) \quad (5)$$

By numerical analysis, we will show later in Section 4 that the above approximation is accurate when the beam size is larger than the detector size. Our derivation of (5) improves the theoretical model of AoA fluctuation-induced link loss. In the previous studies, h_{AoA} is oversimplified in the form of a rectangular function. For example, in [12], $h_{AoA}(\varepsilon) = 0$ (no signal power is detected) for $\varepsilon >$ FoV/2 and $h_{AoA}(\varepsilon) = 1$ (no signal power is loosed) for $\varepsilon <$ FoV/2. In another example, $h_{AoA}(\varepsilon) = h_{AoA}(0)$ (maximum signal power is collected) when $\varepsilon <$ FoV/2 [10].

2.2 Pointing Error-Induced Link Loss

Fig. 1(b) illustrates two scenarios where we have a perfect alignment between the transmitter and the receiver (i.e., no pointing error) and an imperfect alignment (i.e., with pointing error). In this figure, we denote r as the radial displacement between the center of the laser beam at the aperture plane and the receiver aperture. It was shown that Rayleigh distribution fit well with the measured values for pointing error [6]. Thus, the PDF of r can be expressed as

$$PDF_r(r) = \frac{r}{\sigma_r^2} \exp\left(-\frac{r^2}{2\sigma_r^2}\right) \quad (6)$$

where σ_r is the standard deviation of r. We assume a Gaussian beam having the radius of W_a at the aperture plane. Given the radial displacement r, the pointing error-induced link loss can be approximated as [17]

$$h_p(r) \approx \frac{2{A}^2}{W_a^2} \exp\left(-\frac{2r^2}{W_a^2}\right) \quad (7)$$

2.3 PDF and CDF of Link Loss Induced by AoA Fluctuation and Pointing Error

Our objective is to derive the PDF and CDF of link loss induced by AoA fluctuation and pointing error. We express the total link loss arising from two impairments as $h_{ap}(\varepsilon, r) = h_{AoA}(\varepsilon) \times h_p(r)$, assuming that two random variables ε and r are statistically independent. This would be valid especially for FSOC systems operating in the stratosphere since AoA fluctuation mainly arises from the receiver vibration while the pointing error comes from imperfect pointing and vibration of the transmitter. The CDF of total link loss evaluated at a link loss of H can be derived from

$$CDF_{h_{ap}}(H) = \Pr\left(h_{AoA}\, h_{ap} \le H\right) \quad (8)$$

where Pr(.) is the probability that the conditions in the argument satisfy. Substituting (5) and (7) into (8) yields

$$\begin{aligned} CDF_{h_{ap}}(H) &= \Pr\left(\frac{2a^2}{W_d^2} \exp\left(\frac{-2(d_r\varepsilon)^2}{{W_d}^2}\right) \frac{2{A}^2}{W_a^2} \exp\left(\frac{-2r^2}{W_a^2}\right) \le H\right) \\ &= \Pr\left(\alpha\varepsilon^2 + \beta r^2 \ge \log\left(\frac{H}{h_{ap}(0)}\right)\right) \\ &= 1 - CDF_{\kappa}\left(\log\left(\frac{H}{h_{ap}(0)}\right)\right) \end{aligned} \quad (9)$$

where $\alpha = -2d_r^2/W_d^2$, $\beta = -2/W_a^2$, $\kappa = \alpha\varepsilon^2 + \beta r^2$, and $h_{ap}(0) = 2(A/W_a)^2 2(a/W_d)^2$. Now, using the PDFs of ε and r in (1) and (6), we obtain the CDF of κ as

$$CDF_\kappa(\kappa) = \begin{cases} 1 + \frac{\tau_r}{\tau_\varepsilon - \tau_r}\exp(-\tau_\varepsilon\kappa) - \frac{\tau_\varepsilon}{\tau_\varepsilon - \tau_r}\exp(-\tau_r\kappa), & \tau_r \neq \tau_\varepsilon \\ 1 - (1+\tau\kappa)\exp(-\tau\kappa), & \tau_r = \tau_\varepsilon = \tau \end{cases} \tag{10}$$

where $\tau_\varepsilon = 1/(2\alpha\sigma_\varepsilon^2)$ and $\tau_r = 1/(2\beta\sigma_r^2)$. It follows from (9) and (10) that the CDF of link loss induced by AoA fluctuation and pointing error is given by

$$CDF_{h_{ap}}(h_{ap}) = \begin{cases} \frac{\tau_\varepsilon}{\tau_\varepsilon - \tau_r}\exp\left(-\tau_r \log\left(\frac{h_{ap}}{h_{ap}(0)}\right)\right) - \frac{\tau_r}{\tau_\varepsilon - \tau_r}\exp\left(-\tau_\varepsilon \log\left(\frac{h_{ap}}{h_{ap}(0)}\right)\right), & \tau_r \neq \tau_\varepsilon \\ \left(1 + \tau \log\left(\frac{h_{ap}}{h_{ap}(0)}\right)\right)\exp\left(-\tau \log\left(\frac{h_{ap}}{h_{ap}(0)}\right)\right), & \tau_r = \tau_\varepsilon = \tau \end{cases} \tag{11}$$

By taking the derivative of the CDF with respect to h_{ap}, we have an expression about the PDF of h_{ap} as follows

$$PDF_{h_{ap}}(h_{ap}) = \begin{cases} \frac{\tau_\varepsilon \tau_r}{h_{ap}(\tau_r - \tau_\varepsilon)}\left[\exp\left(-\tau_r \log\left(\frac{h_{ap}}{h_{ap}(0)}\right)\right) - \exp\left(-\tau_\varepsilon \log\left(\frac{h_{ap}}{h_{ap}(0)}\right)\right)\right], & \tau_r \neq \tau_\varepsilon \\ -\tau^2 \exp\left(-\tau \log\left(\frac{h_{ap}}{h_{ap}(0)}\right)\right)\log\left(\frac{h_{ap}}{h_{ap}(0)}\right)/h_{ap}, & \tau_r = \tau_\varepsilon = \tau \end{cases} \tag{12}$$

Since the PDF and CDF are fundamental to deriving various performance metrics, they would be helpful to study airborne FSOC systems. In the next Section, we show an example of utilizing the derived CDF for system performance characterization and design optimization.

3. Beam Size Optimization and Adaptation

3.1 Outage Probability and Optimum Beam Sizes

The outage probability, defined as the percentage of time during which the optical power impinging onto the detector is less than the receiver sensitivity, is one of the most important metrics of FSOC system. We consider four factors which affect the performance of FSOC system: channel attenuation, scintillation, AoA fluctuation, and pointing error. We assume that the outage probability of FSOC system operating in the stratosphere is mainly determined by AoA fluctuation and pointing error. Thus, we set the channel attenuation, h_a, to be a constant for a given transmission distance, i.e., $h_a = \exp(-a_c L)$, where a_c is the attenuation coefficient and L is the distance. Also, a system margin of $P_s = P_{sc} + P_{ol}$ is added, where P_{sc} is the system margin to accommodate the effect of scintillation under weak turbulence in the stratosphere (a few decibels, e.g., 4.76 dB as reported in [6]), and P_{ol} is the system margin for optical loss due to diffraction of lenses at transmitter and receiver.

For a transmitter power of P_t, the system outage occurs when the received power P_r is lower than the receiver sensitivity P_{rs}. Thus, the outage probability, P_{out}, can be estimated by

$$P_{out} = \Pr(P_t h_a h_{ap} - P_s \leq P_{rs}) = CDF_{h_{ap}}\left(\frac{P_{rs} + P_s}{P_t h_a}\right) \tag{13}$$

Using (11) and (13), we obtain the outage probability as

$$P_{out} = \begin{cases} \frac{\tau_\varepsilon}{\tau_\varepsilon - \tau_r}\exp\left(-\tau_r \log\left(\frac{P_{rs}+P_s}{P_t h_a h_{ap}(0)}\right)\right) - \frac{\tau_r}{\tau_\varepsilon - \tau_r}\exp\left(-\tau_\varepsilon \log\left(\frac{P_{rs}+P_s}{P_t h_a h_{ap}(0)}\right)\right), & \tau_r \neq \tau_\varepsilon \\ \left(1 + \tau \log\left(\frac{P_{rs}+P_s}{P_t h_a h_{ap}(0)}\right)\right)\exp\left(-\tau \log\left(\frac{P_{rs}+P_s}{P_t h_a h_{ap}(0)}\right)\right), & \tau_r = \tau_\varepsilon = \tau \end{cases} \tag{14}$$

Since we have

$$h_{ap}(0) = \frac{1}{\tau_r \tau_\varepsilon}\left(\frac{Aa}{2d_r \sigma_r \sigma_\varepsilon}\right)^2 \tag{15}$$

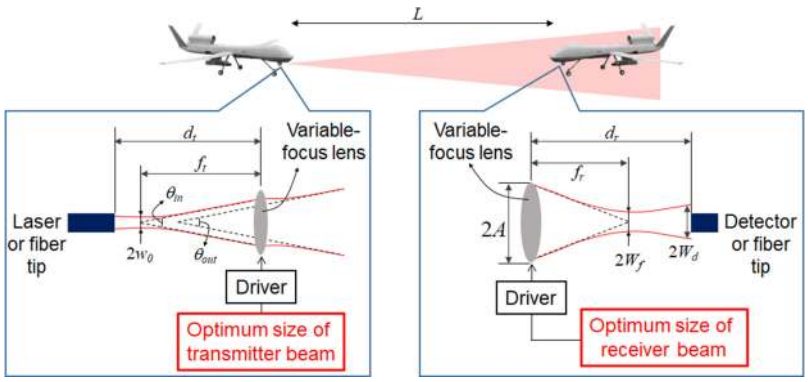

Fig. 2. Proposed adaptive beam control technique.

P_{out} can be expressed as

$$P_{out} = \begin{cases} \frac{\tau_\varepsilon}{\tau_\varepsilon - \tau_r}(k\tau_\varepsilon\tau_r)^{-\tau_r} - \frac{\tau_r}{\tau_\varepsilon - \tau_r}(k\tau_\varepsilon\tau_r)^{-\tau_\varepsilon}, & \tau_r \neq \tau_\varepsilon \\ \left(k\tau^2\right)^{-\tau}\left(1 + \tau\log\left(k\tau^2\right)\right), & \tau_r = \tau_\varepsilon = \tau \end{cases} \tag{16}$$

where $k = (P_{rs} - P_s)/P_t\, h_a (A\, a/2 d_r \sigma_r \sigma_\varepsilon)^2$.

We immediately see the heavy dependence of P_{out} on τ_ε and τ_r. These parameters are beam-size dependent. Therefore, we can optimize the beam sizes for the outage probability. There exists a trade-off between the tolerance to AoA fluctuation and the geometric loss induced by the small detector size compared to the size of focused beam at the receiver: a large size of the focused beam is beneficial for the tolerance to AoA fluctuation, but it increases the geometric loss. Similarly, there exists another trade-off between the tolerance to pointing error and the geometric loss induced by the small receiver-aperture size compared to the beam size at the aperture plane. Thus, our goal can be formulated as finding the minimum outage probability, given a pre-specified value of k. We notice from (16) that P_{out} is a symmetric function of two variables, τ_ε and τ_r. Thus, the optimum value of the function should be at the points $\tau_\varepsilon = \tau_r = \tau$. We, therefore, take the derivative of P_{out} with respect to τ and set it equal to zero. The optimum solutions are $\tau_\varepsilon = \tau_r = -\exp(-1)/k^{1/2}$.

It follows from the expressions about τ_ε and τ_r that the beam sizes that minimize the outage probability can be written as

$$\begin{cases} W_{a,opt} = \sqrt{\frac{0.73 A\, a \sigma_r}{d_r \sigma_\varepsilon}\sqrt{\frac{P_t h_a}{P_{rs} - P_s}}} \\ W_{d,opt} = \sqrt{\frac{0.73 A\, a d_r \sigma_\varepsilon}{\sigma_r}\sqrt{\frac{P_t h_a}{P_{rs} - P_s}}} \end{cases} \tag{17}$$

3.2 Proposed Adaptive Beam Control Technique

Fig. 2 shows the schematic diagram of the proposed adaptive beam control technique. The beam sizes are adjusted to minimize the outage probability. The closed-form expression of (17) allows us to estimate the optimum beam sizes without relying on power-hungry numerical calculations. In the equations, we need the statistical information about AoA fluctuation (σ_ε) and pointing error (σ_r). They could be estimated by analyzing the data on the instantaneous alignment error measured by pointing, acquisition, and tracking (PAT) systems available in airborne platforms. Right after the connection is established, this information as well as other parameters such as location, receiver-aperture size, detector size, receiver sensitivity, transmitter power are exchanged between two airborne platforms. The transmission distance can be estimated from the location information of the two platforms. Thus, the channel attenuation h_a can be estimated from the transmission distance since the channel attenuation coefficient is almost constant in the stratosphere for a given altitude.

From the simple calculation of (17), we can control the beam sizes by adjusting the focal length of lenses, so that beam sizes are set to be $W_{a,op}$ and $W_{d,op}$.

At the transmitter, the light beam is generated by a light source (or at the tip of optical fiber). It then goes through a lens to form the transmitter beam size. The relationship between the properties of the Gaussian beam from the transmitter to the receiver is given by the following equation [20]:

$$W_a = L\,\theta_{out}/2 = L\,\theta_{in}\sqrt{\left(1-\frac{d_t}{f}\right)^2 - \left(\frac{\pi w_0^2}{\lambda f}\right)^2}\,/2 \tag{18}$$

where L is the link distance, θ_{in} and θ_{out} are the beam divergence angles before and after lenses, respectively, w_o is the initial beam radius (at the light source), d_t is the distance between the light source and lens, and f_t is the focal length of the transmitter lens. The initial beam divergence angle is given by $\theta_{in} = 2\lambda/\pi w_o$, depending upon only the light source. Also, the distance between the light source and lens, d_t, is fixed in our design. Given w_o, λ and d_t, W_a can be adjusted by changing the focal length f_t.

At the receiver, the light beam impinges onto the circular aperture. An Airy pattern describes the collected spot of light on the detector plane. Note that, the position of detector plane is fixed at a distance d_r from the aperture, while the position of focal plane can be adjusted by changing the beam size. Due to the fact that the Airy pattern can be approximated by a Gaussian beam, the relationship between the beam sizes on the detector and focal planes is dictated by the following equation:

$$W_d = W_f\sqrt{1+\left(\frac{d_r - f}{z_R}\right)^2} \tag{19}$$

where $W_f = 0.42\lambda f_r/2\,\mathrm{A}$ is the equivalent Gaussian beam radius on the focal plane [19] and $z_R = \pi W_f^2/\lambda$ is the Rayleigh range [21]. Given A, λ and d_r, W_d can be adjusted by changing the focal length f_r.

An electrically focus-tunable lens can be used to adjust the focal length without changing the position of optical components at the transmitter and receiver. This lens can be implemented by using a variety of techniques, such as voltage-controlled shape or voltage-controlled refractive index [22].

4. Results and Discussions

In this section, the performance analysis and improvement of FSOC systems are numerically evaluated by using Monte-Carlo computer simulation. We first discuss the validity of all derived expressions, including the Gaussian approximation of AoA fluctuation-induced loss, probability density functions of link loss, outage probability, and optimum beam sizes. Then, we evaluate the effectiveness of the proposed adaptive beam control technique.

We consider a receiver having $a = 4.5\ \mu$m (SMF) and $d_r = 3\,$cm. The root mean square error (RMSE) between the exact (3) and the approximate (5) expressions for $h_{A\,oA}$ is shown in Fig. 3 for different values of W_d/a. When the beam size (W_d) increases, our analysis based on Gaussian approximation agrees well with (3). This is because the Gaussian approximation ignores the relatively small outer rings of the Airy pattern and estimates its main lobe. The results show that our simple expression of (5) is in good agreement with (3) when W_d/a is larger than 2, where RMSE $< 10^{-2}$.

Next, we provide and compare the PDF and CDF of link loss (h_{ap}) obtained from our theory and Monte Carlo simulations for different values of standard deviation of AoA fluctuation (σ_ε) and for different values of standard deviation of pointing error (σ_r) in Figs. 4 and 5. The parameters in both figures are as follows: $2W_a = 4\,$m, $2W_d = 19\,\mu$m, $A = 1.5$ cm. We also set $\sigma_r = 50\,$cm and $\sigma_\varepsilon = 100\ \mu$rad in Figs. 4 and 5, respectively. For simulations, each line is calculated by generating 1,000,000 independent cases of AoA fluctuation and pointing error. Rayleigh distributions are utilized in the simulation to generate those cases. We observe that our derived CDF and PDF

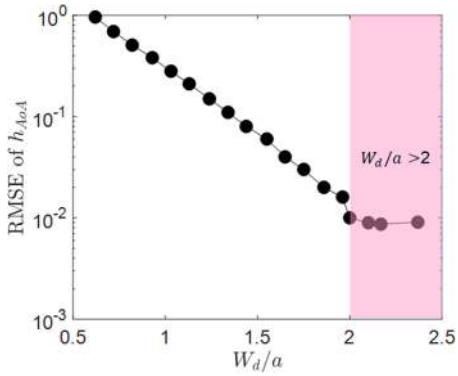

Fig. 3. Accuracy of AoA fluctuation-induced loss estimation as a function of receiver beam size.

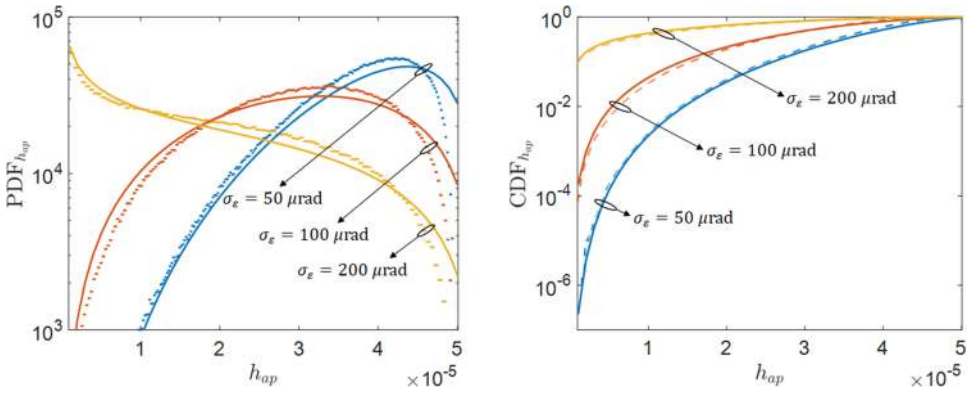

Fig. 4. PDF and CDF obtained from simulations (dotted lines) and theoretical derivations (solid lines) for different standard deviations of AoA fluctuation (σ_ε).

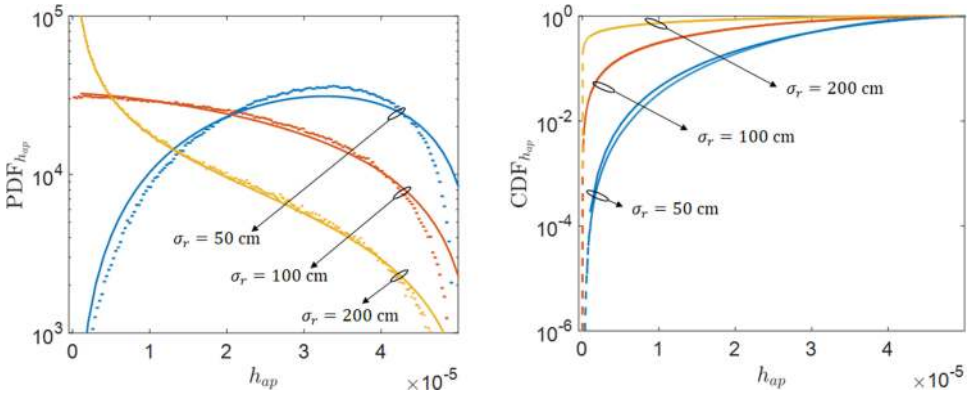

Fig. 5. PDF and CDF obtained from simulations (dotted lines) and theoretical derivations (solid lines) for different standard deviations of pointing error (σ_r).

expressions are very close to results obtained from the simulation. This confirms the correctness of our derivations. Moreover, the larger the AoA fluctuation and pointing error, the better match between analysis and simulation is observed. Therefore, the proposed PDF and CDF expressions would be particularly applicable to airborne FSOC systems, where the variances of alignment error are typically large.

TABLE 1
Parameters of Airborne FSOC System

Symbol	Quantity	Value
P_t	transmitted power	25 dBm
λ	wavelength	1550 nm
w_o	initial beam radius	5.25 μm
P_{rs}	receiver sensitivity	-38.9 dBm
$2A$	aperture diameter	30 mm
$2a$	detector diameter	9 μm (SMF)
d_r	lens to detector distance	3 cm
L	link distance	100 km
a_c	attenuation coefficient	3.5×10^{-6} km^{-1}
P_{sc}	system margin for scintillation	4.76 dB
P_{ol}	system margin for optical loss	2.2 dB (Tx), 2.2 dB (Rx)

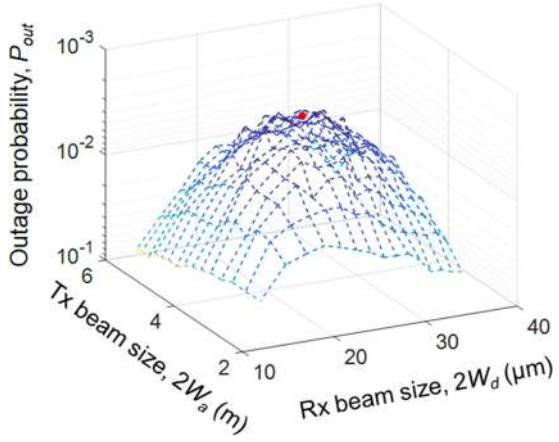

Fig. 6. Outage probability as functions of transmitter and receiver beam sizes obtained by simulations (mesh grid) and optimum beam sizes obtained from theoretical expressions (red dot).

In Section 3, we showed an example of applying the CDF expression to improve the system performance and provided the closed-form expressions about optimum beam sizes for the outage probability. To verify the expressions, we evaluate the outage probability for an airborne FSOC system using numerical simulation. The system parameters are shown in Table 1. We set the receiver sensitivity to be -38.9 dBm, assuming to employ an avalanche photo-detector with a sensitivity of 1000 photon/bit at 1 Gb/s. Some parameters for link budget calculation are similar to the ones reported in [6]. Fig. 6 shows the outage probability of 100-km FSOC link when $\sigma_\varepsilon = 100\,\mu$rad and $\sigma_r = 50$ cm. The result contains a grid of 225 points, where each of them is calculated by the simulation with 10,000 independent cases of AoA fluctuation and pointing error generated. The simulation results show that the optimum beam sizes for outage probability are found to be $2W_{d,opt} = 24\,\mu$m and $2W_{a,opt} = 4$ m. We also estimate the optimum beam sizes using (17). They are estimated to be $2W_{d,opt} = 23.2\,\mu$m and $2W_{a,opt} = 3.88$ m (shown as the red point in the figure), which agree very well with the ones found by using the computer simulation. It is worth mentioning that it takes 0.94 hours to obtain these values through computer simulation, whereas our closed-form expressions yield the results in 21 μs (by using the same computer). It clearly shows that the simple, closed-form solutions are useful for saving the computation time and power required for the system optimization.

Figs. 7 and 8 show the outage probability versus the standard deviations of AoA fluctuation (when $\sigma_r = 50$ cm) and pointing error (when $\sigma_\varepsilon = 100\,\mu$rad), respectively. The results are obtained

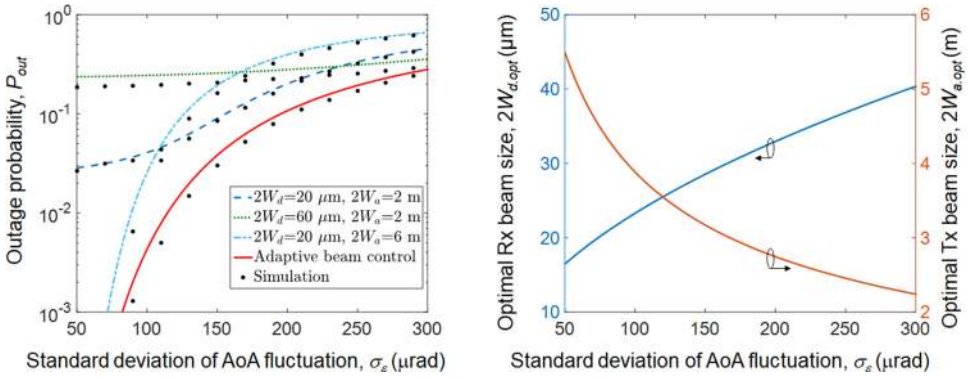

Fig. 7. Outage probability and optimal beam sizes as a function of standard deviation of AoA fluctuation (σ_ε).

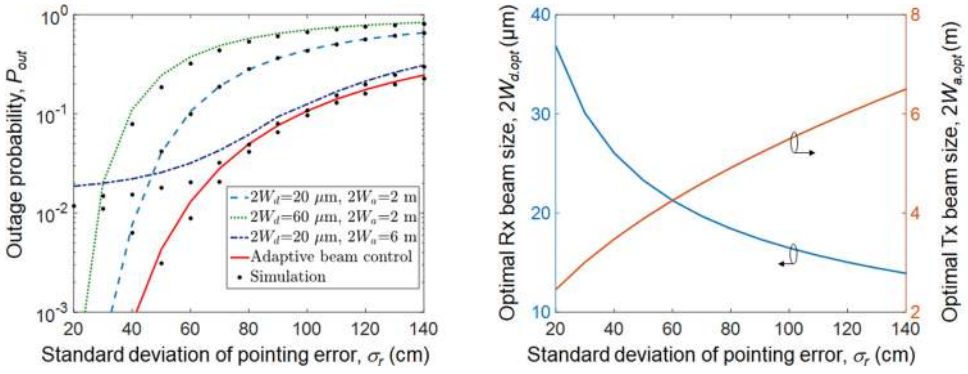

Fig. 8. Outage probability and optimal beam sizes as a function of standard deviation of pointing error (σ_r).

by using the theoretical analysis of (16) and the simulation. The simulation results agree well with the values calculated from our theory. In Fig. 7, a small receiver beam size ($2W_d = 20\,\mu$m) helps to maintain low outage probabilities in the case of small AoA fluctuation, but it results in relatively high outage probabilities when AoA fluctuation is large. On the other hand, a large receiver beam size ($2W_d = 60\,\mu$m) maintains low outage probabilities over a wide range of large AoA fluctuations, but it leads to high outage probabilities when AoA fluctuation is small. Fig. 8 shows that the narrow transmitter beam size ($2W_a = 2$ m) is preferable when the pointing error is low. However, as the pointing error increases (e.g., $\sigma_r > 45$ cm), a large transmitter beam size ($2W_a = 6$ m) is a better choice. From both figures, it is clear that none of the combinations of fixed beam sizes can provide good performance over a wide range of alignment errors.

By adopting the proposed adaptive control technique at the transmitter and receiver, we can achieve the minimum outage probability over wide ranges of AoA fluctuation and pointing error, as shown in Figs. 7 and 8. This is because when the conditions for alignment error change, the beam sizes at both transmitter and receiver should be adjusted accordingly. We also show in these figures the optimal beam sizes to realize the adaptive beam control technique. The results show that as the standard deviation of AoA fluctuation increases (given a fixed σ_r), we should enlarge the receiver beam size, and at the same time narrow the transmitter beam size. This is because a wider beam size is needed at the receiver to reduce the link loss induced by AoA fluctuation, and a narrower beam size at the transmitter is required to reduce the geometric loss. In contrast, as the standard deviation of pointing error increases (given a fixed σ_ε), we should increase the transmitter beam size, and reduce the receiver beam size: a wider transmitter beam size is preferable to reduce the

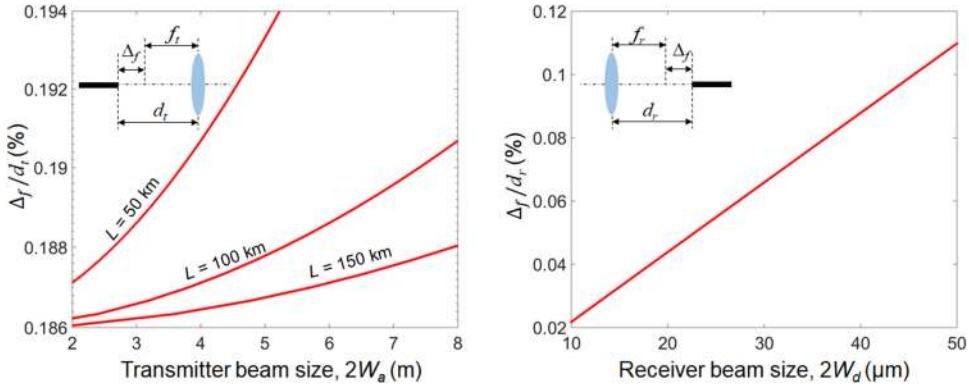

Fig. 9. Variable focal ranges of transmitter and receiver lens.

link loss induced by pointing error in this case, and a narrower receiver beam size should be utilized to make the beam better focused in the detector plane.

Finally, we present the properties of the variable-focus lens setup to realize the adaptive beam control technique in Fig. 9. For the ranges of alignment errors, 50 μrad $<\sigma_\epsilon<$ 300 μrad and 20 cm $<\sigma_r<$ 140 cm, the overall ranges required for beam sizes are approximately, 10 μm $< 2W_d <$ 50 μm and 2 m $< 2W_a <$ 8 m. For the lens operation, the input values for the lens controllers are specified in the figure. More specifically, to increase (or decrease) the beam size, at both transmitter and receiver, we can simply decrease (or increase) the value of focal length. In the figure, Δ_f is the distance between (i) the focal plane and the detector plane (at the receiver), or (ii) the focal plane and the light-emitting plane (at the transmitter). The operation range of the focal length is (i) $d_t - \Delta_f$, where 0.186% $< \Delta_f/d_t <$ 0.191% for the transmitter lens (when $L =$ 100 km), and (ii) $d_r - \Delta_f$, where 0.02% $< \Delta_f/d_r <$ 0.12% for the receiver lens. These ranges are calculated by using (18) and (19). It is noted that the operation range of transmitter focal length is also dependent on the link distance. For a longer distance, a shorter range is needed, e.g., 0.186% $<\Delta_f/d_t<$ 0.188% (when $L =$ 150 km). This is due to the fact that the transmitter beam size is linearly proportional to the distance. It implies that to realize the adaptive beam control technique, especially for long distances, the lenses with a limited variable-focus range are acceptable, thus improving the possibility to implement the technique in practice. However, a high-resolution controller is needed to realize such small changes of focus. That can be done by high precise voltage-controlled systems. It is important to note that similar results can be obtained for other communication scenarios and systems to design the transceiver lens.

5. Conclusions

We have presented the closed-form expressions about the probability density function and cumulative density function of link loss induced by AoA fluctuation and pointing error. Using these expressions, we have derived the closed-form expressions about the outage probability of FSOC systems operating at high altitudes. Monte Carlo simulations were carried out validate our analytical derivations.

We have also proposed a non-mechanical and energy-efficient adaptive beam control technique to mitigate the adverse effects of AoA fluctuation and pointing error. By utilizing the focus-variable lenses and closed-form expressions about the beam sizes, we can minimize the outage probability of airborne FSOC systems without bulky mechanical positioning systems and time-consuming calculations required for the optimization.

The theoretical analyses conducted in this paper would be useful for characterizing the system performance and designing the airborne FSOC systems. Also, the proposed adaptive beam control

technique could be an effective method to improve the performance airborne FSOC systems having tight constrains on size, weight, and power.

References

[1] F. Fidler, M. Knapek, J. Horwath, and W. R. Leeb, "Optical communications for high-altitude platforms," *IEEE J. Sel. Topics Quantum Electron.*, vol. 15, no. 5, pp. 1058–1070, May 2010.
[2] M. Alzenad, M. Z. Shakir, H. Yanikomeroglu, and M. S. Alouini, "FSO-based vertical backhaul/fronthaul framework for 5G+ wireless networks," *IEEE Commun. Mag.*, vol. 56, no. 1, pp. 218–224, Jan. 2018.
[3] W. Fawaz, C. A. Rjeily, and C. Assi, "UAV-aided cooperation for FSO communication systems," *IEEE Commun. Mag.*, vol. 56, no. 1, pp. 70–75, Jan. 2018.
[4] Y. Kaymak, R. R. Cessa, J. Feng, N. Ansari, M. C. Zhou, and T. Zhang, "A survey on acquisition, tracking, and pointing mechanisms for mobile free-space optical communications," *IEEE Commun. Surv. Tuts.*, vol. 20, no. 2, pp. 1104–1123, Feb. 2018.
[5] C. Chen *et al.*, "High-speed optical links for UAV applications," *Proc. SPIE*, vol. 10096, 2017, Art. no. 1009615.
[6] B. Moision *et al.*, "Demonstration of free-space optical communication for long-range data links between balloons on project loon," *Proc. SPIE*, vol. 10096, 2017, Art. no. 100960Z.
[7] M. A. Khalighi and M. Uysal, "Survey on free space optical communication: a communication theory perspective," *IEEE Surveys Tuts.*, vol. 16, no. 4, pp. 2231–2258, Jun. 2014.
[8] H. Kaushal and G. Kaddoum, "Optical communication in space: challenges and mitigation techniques," *IEEE Surveys Tuts.*, vol. 19, no. 1, pp. 57–96, Aug. 2017.
[9] E. Ciaramella *et al.*, "1.28 terabit/s (32 $\times$ 40 Gbit/s) WDM transmission system for free space optical communications," *IEEE J. Sel. Areas Commun.*, vol. 27, no. 9, pp. 1639–1645, Dec. 2009.
[10] S. Huang and M. Safari, "Free-space optical communication impaired by angular fluctuations," *IEEE Trans. Wireless Commun.*, vol. 16, no. 11, pp. 7475–7487, Sep. 2017.
[11] X. Ke and Z. Tan, "Effect of angle-of-arrival fluctuation on heterodyne detection in slant atmospheric turbulence," *Appl. Opt.*, vol. 57, no. 5, pp. 1083–1090, Feb. 2018.
[12] M. T. Dabiri, S. M. S. Sadough, and M. A. Khalighi, "Channel modeling and parameter optimization for hovering UAV-based free-space optical links," *IEEE J. Sel. Areas Commun.*, vol. 36, no. 9, pp. 2104–2113, Oct. 2018.
[13] H. Takenaka, M. Toyoshima, and Y. Takayama, "Experimental verification of fiber-coupling efficiency for satellite-to-ground atmospheric laser downlinks," *Opt. Exp.*, vol. 20, no. 14, pp. 15301–15308, Jun. 2012.
[14] R. Zhang, J. Wang, G. Zhao, and J. Lv, "Fiber-based free-space optical coherent receiver with vibration compensation mechanism," *Opt. Exp.*, vol. 21, no. 15, pp. 18434–18441, Jul. 2013.
[15] G. Huang, C. Geng, F. Li, Y. Yang, and X. Li, "Adaptive SMF coupling based on precise-delayed SPGD algorithm and its application in free space optical communication," *IEEE Photon. J.*, vol. 10, no. 3, Jun. 2018, Art. no. 7904212.
[16] T. Song, Q. Wang, M. W. Wu, and P. Y. Kam, "Performance of laser inter-satellite links with dynamic beam waist adjustment," *Opt. Exp.*, vol. 24, no. 11, pp. 11950–11960, May 2016.
[17] V. V. Mai and H. Kim, "Adaptive beam control techniques for airborne free-space optical communication systems," *Appl. Opt.*, vol. 57, no. 26, pp. 7462–7471, Sep. 2018.
[18] V. V. Mai and H. Kim, "Mitigation of effects of angle-of-arrival fluctuation and pointing error on airborne free-space optical systems," in *Proc. Opt. Fiber Commun.*, San Francisco, CA, USA, Mar. 2019, paper W2A.40.
[19] B. Zhang, J. Zerubia, and J. C. O. Marin, "Gaussian approximations of fluorescence microscope point-spread function models," *Appl. Opt.*, vol. 46, no. 10, pp. 1819–1829, Sep. 2007.
[20] CVI Mellets Griot, "Gaussian beam optics," CVI Melles Griot Tech. Guide, vol. 2, pp. 1–14, 2009.
[21] R. Paschotta, *Field Guide to Lasers*. Bellingham, WA, USA: SPIE Press, 2008, pp. 1–126.
[22] H. Ren and S. T. Wu, "Variable-focus liquid lens," *Opt. Exp.*, vol. 15, no. 10, pp. 5931–5936, Apr. 2007.